J. Fluid Mech. (2001), *vol.* 445, *pp.* 285–303.
DOI: 10.1017/S0022112001005614 Printed in the United Kingdom

Stability and transition of stratified natural convection flow in open cavities

By A. JAVAM AND S. W. ARMFIELD

Department of Mechanical Engineering, University of Sydney, Sydney, 2006, Australia

(Received 4 April 1999 and in revised form 19 March 2001)

In this study we have investigated the behaviour of natural convection flow in open cavities, with both homogeneous and thermally stratified ambient, using direct numerical simulation. The cavity is insulated at the top and bottom boundaries, heated from the left-hand side boundary and open at the right-hand side. A wide range of Rayleigh numbers were considered (5×10^6 to 1×10^{10}) with $Pr = 0.7$ for all cases. It was found that the homogeneous flow is steady for all Rayleigh numbers considered, whereas the stratified flow with a high enough Rayleigh number exhibits low- and high-frequency signals of the same type as are observed for closed cavity flow. The thermal boundary layer is examined in detail and it is shown that both low- and high-frequency signals are located predominantly in the upper region of the heated plate and are associated with a reverse-S-flow formed by the boundary layer exit jet interacting with the stratified interior. The low-frequency signal is associated with standing waves in the boundary layer, whereas the high-frequency signal is associated with travelling waves. The high-frequency signal occurs initially as a harmonic of the base low-frequency signal. A corner jet with the same inlet characteristics as the natural convection boundary layer exit jet is also examined and shown to exhibit a similar bifurcation, but with the low frequency always dominant. It is suggested that the generation mechanism for the bifurcation of the natural convection flow is the same as that for the corner jet.

1. Introduction

Natural convection in enclosed cavities has received considerable attention because of its fundamental importance in the understanding of buoyancy-driven flows and its wide range of engineering applications. Natural convection in a cavity with one vertical side open has received much less attention even though it also has a wide range of industrial applications and embodies much of the fundamental fluid mechanics of the enclosed cavity. Some applications are refrigerators and ovens in open door conditions, solar thermal receiver systems, thermosyphons, fire spread in buildings, natural convection cooling of electronic devices, brake-housing systems in aircraft, and pipes joining reservoirs and oceans. In many of these cases the ambient fluid is stratified.

In the enclosed square cavity the left- and right-hand walls are heated and cooled respectively, with the top and bottom boundaries insulated, generating natural convection boundary layers travelling up and down the hot and cold walls discharging intrusions into the interior of the cavity. For steady or quasi-steady flow the interior of the cavity is stratified and, for square cavities, contains a single cavity-scale circulation transferring heated fluid from the hot to the cold wall at the top of the cavity, and cooled fluid from the cold to the hot wall at the bottom of the cavity. In

the heated open cavity the cold wall is replaced with an open boundary. The heated fluid discharged by the hot wall travels across the upper part of the cavity and exits through the upper part of the open boundary. Ambient fluid is entrained across the remainder of the open boundary, travels across the cavity and is entrained by the boundary layer.

It is well known that natural convection flow in closed square cavities at Prandtl number $Pr = 0.7$ undergoes a bifurcation to time-periodic flow when the Rayleigh number is greater than a critical value (LeQuere & Alziary de Roquefort 1985; Paolucci & Chenoweth 1989). In a closed square cavity the bifurcation occurs at approximately Rayleigh number $Ra = 0.875 \times 10^8$, where the Rayleigh number is based on the temperature difference in the boundary layer. This definition of the Rayleigh number has been chosen as appropriate for the open cavity flow. Rayleigh numbers for the closed cavity are often expressed in terms of the total temperature difference, giving a Rayleigh number twice as large as that based on the boundary layer temperature difference. As the Rayleigh number is increased a second, higher-frequency signal appears at approximately $Ra = 1.375 \times 10^8$. The bifurcation signal has approximately the characteristic frequency of the internal waves (Janssen & Henkes 1995), while the second, higher frequency has approximately the characteristic frequency of the boundary layer (Janssen & Armfield 1996). LeQuere & Behnia (1998) showed that the bifurcation in the closed cavity must be asymmetric, breaking the skew symmetry of the base flow.

The generation mechanism for the absolute instabilities that give rise to these bifurcation signals is not fully understood. The boundary layer exit flow is similar to a Bickley jet, which is known to exhibit a Kelvin–Helmholtz instability with a character similar to that of the low frequency in the cavity, and it has been suggested that this is the generation mechanism for the bifurcation and low-frequency signal (Janssen & Henkes 1995). The natural convection boundary layer on a semi-infinite flat plate with isothermal ambient is convectively unstable above a critical Rayleigh number, so that if a perturbation is continually applied to the flow a train of waves will travel away from the location of the perturbation, amplifying in their direction of travel. The convective character of the instability means that once the perturbation ceases the waves travel out of the system and also cease (Armfield & Patterson 1992; Armfield & Janssen 1996; Janssen & Armfield 1996). The critical Rayleigh number for the convective instability of the boundary layer, at $Pr = 0.7$, is approximately $Ra = 1 \times 10^5$. It has been suggested that the boundary layer signal seen in the closed cavity for high enough Rayleigh number is a result of this known instability, with a much higher critical Rayleigh number as a result of the influence of the stratification of the interior fluid. This hypothesis was supported by the work of Gill & Davey (1969), in which the stability of natural convection flow in a semi-infinite vertical slot with stratified walls and ambient was analysed, and critical Rayleigh numbers comparable to that of the cavity bifurcation obtained. Recent work has shown that the natural convection boundary layer in the fully developed cavity flow has a critical Rayleigh number and stability characteristics very close to those of the semi-infinite plate with an isothermal ambient and therefore the Gill & Davey result cannot be applied to the cavity boundary layer flow (Janssen & Armfield 1996). It is therefore unlikely that the critical Rayleigh number for the occurrence of the boundary layer frequency signal in the cavity (approximately 1.375×10^8) can be related directly to the critical Rayleigh number for the boundary layer instability, which is several orders of magnitude less (approximately 1.0×10^5). Additionally, as noted above, the boundary layer is convectively unstable, whereas the cavity signal is the result of an

absolute instability which does not require the continual imposition of an external perturbation, further indicating that the second cavity frequency is not a result of the boundary layer instability alone.

Ravi, Henkes & Hoogendoorn (1994) also investigated the closed cavity flow, concentrating on the flow structure that forms at the downstream corners of the thermal boundary layers. At high values of the Rayleigh number a recirculation pocket appears near the corners downstream of the vertical walls, and the flow separates and reattaches to the horizontal walls in the vicinity of this recirculation with a considerable thickening of the horizontal layers. This corner flow was considered by some previous researchers to be an internal hydraulic jump and jump theory was used to predict bifurcation of the steady flow into periodic flow. However, Ravi *et al.*'s (1994) study revealed that the corner flow does not have the characteristics of a conventional hydraulic jump. The present work examines this corner flow, which takes the form of a reverse S-shape, in the context of the open cavity, and explores the link between this phenomenon, stratification, Rayleigh number and bifurcation.

Previous investigations of open cavity flow have been primarily concerned with determining overall flow and heat transfer features, and have not observed a bifurcation of the type described above for closed cavity flow. Early theoretical studies were those of Lighthill (1953) and Hartnett & Welsh (1957). Much of the work prior to 1973 has been summarized in Japikse (1973). Bejan & Kimura (1981) conducted a theoretical and experimental investigation and demonstrated that Ra must exceed 1.2×10^3 for the free convection to penetrate laterally to a length greater than the cavity height. Penot (1982) used a streamfunction–vorticity method with the Boussinesq approximation to study an open cavity with three heated sides. Le Quere, Humphrey & Sherman (1981) used the same configuration, dispensing with the Boussinesq approximation and employing primitive variables. Chan & Tien (1985) studied an open shallow cavity with aspect ratio of 0.143 and Rayleigh numbers ranging from 10^6 to 10^7 under steady laminar conditions. Their results indicated that the rate of heat transfer approaches that for a vertically heated flat plate and that natural convection inside the cavity is not much influenced by the far field. Steady-state fluid flow and heat transfer in cavities with the top boundary open and bottom boundary heated was investigated numerically by Mohamad (1995) for different angles, aspect ratios and Rayleigh numbers varying from 10^3 to 10^7. It was found that for high enough Rayleigh number the flow exhibits instabilities at high Rayleigh numbers and low inclination angles resulting from the unstable stratification that is established when the heated wall is on the bottom.

None of the open cavity flow investigations cited above considered stratified open cavity flow. In this paper we will present results obtained for open cavity natural convection flow with both homogeneous and stratified ambient at Prandtl number $Pr = 0.7$. As has been observed in the previous investigations the homogeneous ambient flow does not exhibit bifurcation. In the present study it has been found that the flow with stratified ambient does exhibit a bifurcation with a similar character to that observed in the closed cavity at the same Prandtl number. Further investigation of the open cavity bifurcation, together with the reverse-S flow, the natural convection boundary layer in isolation and a horizontal buoyant corner jet with the characteristics of the boundary layer exit jet, have allowed considerable additional insight into the character of the bifurcation obtained. In particular it is shown that both the characteristic frequencies are associated with the turning flow that arises at the top of the heated wall for the stratified flow and both are generated by an instability of the boundary layer exit jet.

2. Mathematical model

Two-dimensional motion of an incompressible and viscous fluid in a rectangular cavity with a background stratification is governed by the conservation of momentum, heat and volume. These equations, under the Boussinesq approximation, can be expressed in non-dimensional form as follows:

$$\frac{\partial u}{\partial t} + u\frac{\partial u}{\partial x} + v\frac{\partial u}{\partial y} = -\frac{\partial p}{\partial x} + \left(\frac{\partial^2 u}{\partial x^2} + \frac{\partial^2 u}{\partial y^2}\right), \tag{2.1}$$

$$\frac{\partial v}{\partial t} + u\frac{\partial v}{\partial x} + v\frac{\partial v}{\partial y} = -\frac{\partial p}{\partial y} + \left(\frac{\partial^2 v}{\partial x^2} + \frac{\partial^2 v}{\partial y^2}\right) + \frac{Ra}{Pr}(T), \tag{2.2}$$

$$\frac{\partial T}{\partial t} + u\frac{\partial T}{\partial x} + v\frac{\partial T}{\partial y} = \frac{1}{Pr}\left(\frac{\partial^2 T}{\partial x^2} + \frac{\partial^2 T}{\partial y^2}\right) - v\frac{\mathrm{d}T_b}{\mathrm{d}y}, \tag{2.3}$$

$$\frac{\partial u}{\partial x} + \frac{\partial v}{\partial y} = 0, \tag{2.4}$$

where

$$Pr = \frac{v}{\kappa}, \qquad Ra = \frac{g\beta\Delta T H^3}{v\kappa}, \tag{2.5}$$

and where u and v are the velocity components in the x- and y-directions respectively, t is the time, T and T_b are the fluctuating and background temperature respectively, with T_b a function of y only. The total temperature is $T + T_b$; β, κ and v are the coefficients of thermal expansion, thermal conductivity and kinematic viscosity respectively, g is the acceleration due to gravity and H is the height of the cavity. Lengths are non-dimensionalized by the height of the cavity H, the temperature relative to the mean temperature by ΔT, and time by H^2/v. ΔT is the dimensional difference between the total temperature on the heated wall and the background temperature at the height at which the non-dimensional background temperature is set to zero. The total temperature will be referred to as the temperature in the rest of the paper.

The equations of motion (2.1)–(2.4) were solved using a fractional-step Navier–Stokes solver. The scheme is defined on a non-staggered mesh, in which all the variables are stored at the same grid locations, using finite volumes, with standard second-order central differences used for the viscous terms, the pressure gradient and divergence terms. The advective terms are approximated using QUICK (Leonard 1979). The momentum and temperature equations are inverted using a limited iteration ADI solver and the Poisson pressure correction equation uses a preconditioned restarted GMRES solver. The scheme is similar to that presented for a staggered mesh in Armfield & Street (1999).

The computational domain, together with boundary conditions for the fixed boundaries, is shown in figure 1. With a finite-volume scheme an additional node is included outside the domain and for Dirichlet boundary conditions the average of the dependent variable at the exterior and immediate interior nodes is set to the required value. For Neumann boundary conditions the gradient in finite difference form using the dependent variable at the exterior and immediate interior nodes is set to the required value.

On the open boundary the normal gradient of vertical and horizontal velocity is set to zero. The horizontal gradient of fluctuating temperature is set to zero in the

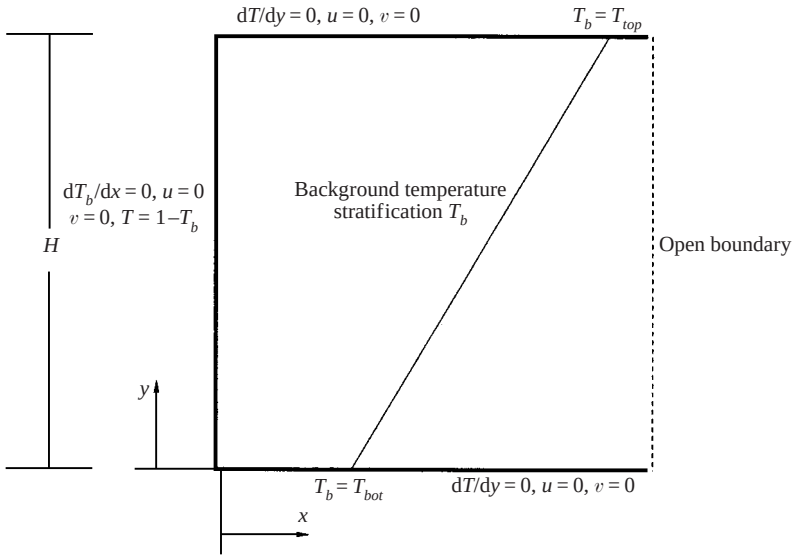

FIGURE 1. Schematic presentation of the computational domain.

outflow region, that is where the horizontal velocity is positive on the boundary, while in the inflow region where the horizontal velocity on the open boundary is negative, the fluctuating temperature is set to zero.

A non-uniform mesh is used allowing grid nodes to be concentrated in regions of rapid solution variation, adjacent to the heated plate and the upper and lower boundaries. The origin lies at the bottom left corner of the domain with y increasing up the heated plate and x increasing horizontally into the domain. The horizontal mesh size adjacent to the heated wall is $\Delta x = 0.002$ with a grid stretching factor of 1.08 per cell until $x = 0.2$, after which the stretching factor is gradually reduced until the grid becomes uniform in the interior. The vertical mesh size adjacent to the upper and lower boundaries is $\Delta y = 0.002$ with again a grid stretching factor of 1.08 per cell until $y = 0.2$ for the lower domain and $y = 0.8$ for the upper domain, after which the stretching factor is gradually reduced until the grid becomes uniform in the interior, resulting in a mesh of 59×97 nodes. The time step used was $\Delta t = 5 \times 10^{-7}$.

Time-step-dependence tests were carried out by obtaining additional results at half the time step given above. The variation in the amplitude of the bifurcated modes was found to be less than 2%, while there was no discernible difference in the frequencies. Mesh-dependence tests have also been carried out by halving the mesh size at the heated wall and upper and lower boundaries, halving the stretching factor and halving the time step. Again the solutions on the two meshes showed a less than 2% variation with no discernible difference in the frequencies and other features of the bifurcation.

To determine any effect of the cavity aspect ratio and open boundary condition simulations were also carried out in a cavity with twice the horizontal length and the same grid spacings given above, resulting in an 86×97 grid. This led to a less than 3% change in the lateral temperature profile in the boundary layer, the most sensitive quantity in the solution. The occurrence of the bifurcations and other quantitative features of the two flows were identical.

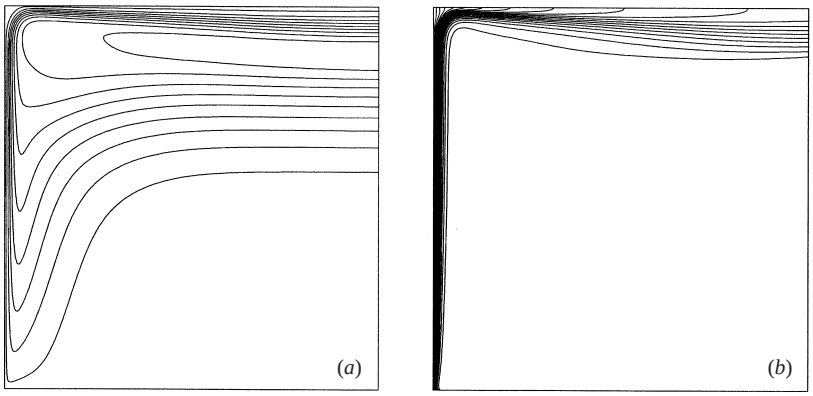

FIGURE 2. Streamfunction (*a*) and temperature (*b*) contour plots for zero background stratification at $Ra = 0.5 \times 10^8$.

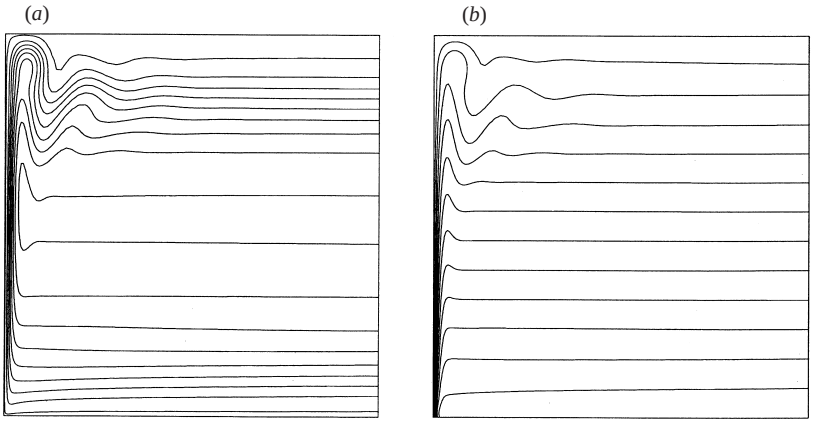

FIGURE 3. Streamfunction (*a*) and temperature (*b*) contour plots for flow with background stratification at $Ra = 0.5 \times 10^8$.

3. Results

Results have been obtained for Ra ranging from 5×10^6 to 1×10^{10}, with $Pr = 0.7$, in a square open cavity. The cavity is initially filled with a quiescent fluid. At time $t = 0$ the left-hand wall is instantaneously heated to a non-dimensional temperature of 1.0 and the flow allowed to develop. Flows with both homogeneous and stably stratified ambients have been considered. In the stratified case, the background stratification gradient is constant ($\mathrm{d}T_b/\mathrm{d}y = 2$), with $T_{top} = 1$. The flow with homogeneous ambient has $T_b = 0$. For all flows considered, by time $t = 0.05$ a quasi-steady flow has developed.

Figure 2 contains the streamfunction and temperature contours for the flow with zero stratification at time $t = 0.06$ and $Ra = 0.5 \times 10^8$, with the heated wall on the left facing the open boundary on the right. A thermal boundary layer has developed, travelling up the heated wall, entraining ambient fluid from the cavity over the lower 90% of its height. This fluid is discharged as a heated wall jet that travels across the cavity immediately beneath the upper boundary and exits through the open boundary without any significant change in character. By this stage of development the flow is steady and no bifurcation is observed.

Figure 3 contains the streamfunction and temperature contours for the stratified

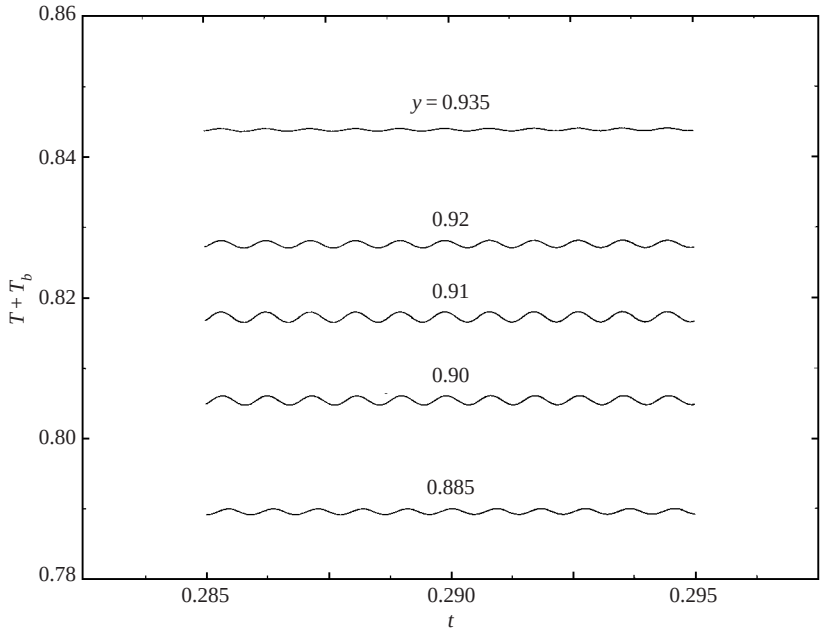

FIGURE 4. Time series of temperature at $x = 1/120$ for the stratified flow at $Ra = 0.825 \times 10^8$.

flow at time $t = 0.06$ and $Ra = 0.5 \times 10^8$. Again a thermal boundary layer has developed that travels up the heated wall, with ambient fluid now entrained over only the lower half of its height, and discharged over the upper half. A component of the discharge forms a boundary layer exit jet at the downstream corner that almost immediately turns down into the cavity, and then rises again to form a tight reverse-S-shaped structure. The jet then spreads out to form a gravity intrusion with vertical extent several times that of the initial jet. At this Rayleigh number the stratified flow is also steady; however the character of the exit jet and intrusion is completely different to that of the non-stratified flow.

At $Ra = 0.825 \times 10^8$ it is observed that the stratified flow is no longer steady at large time but exhibits wave-like behaviour. Figure 4 shows temperature time series at $x = 1/120$ and a range of vertical locations inside the thermal boundary layer, adjacent to the upper part of the heated wall. The sinusoidal behaviour of the time series clearly demonstrates the unsteadiness of the flow. Spectra of the time series at $y = 0.91$ are shown in figure 5(a), where it is seen that the dominant mode has a frequency $f = 1100$.

As the Rayleigh number of the stratified flow is further increased additional modes appear. Figure 5(b) shows the spectrum for the time series at $y = 0.91$ for Rayleigh number $Ra = 0.875 \times 10^8$. A peak is seen at $f_1 = 1139$, which corresponds to the $f = 1100$ mode observed at the lower Rayleigh number. However at this Rayleigh number additional higher frequency modes are observed, some having amplitudes greater than that of the base $f_1 = 1139$ mode. The dominant mode now occurs at $f_2 = 5600$, which is approximately $5 \times f_1$. The remaining higher frequency modes are all integer multiples of the base mode, as labelled on figure 5(b). Increasing the Rayleigh number further to $Ra = 1.0 \times 10^8$ increases the base mode to $f_1 = 1275$ and the dominant high-frequency mode to $f_2 = 5936$, as shown in figure 5(c). For this Rayleigh number $f_2 = 4.66 f_1$ and additional harmonics and sub-harmonics of

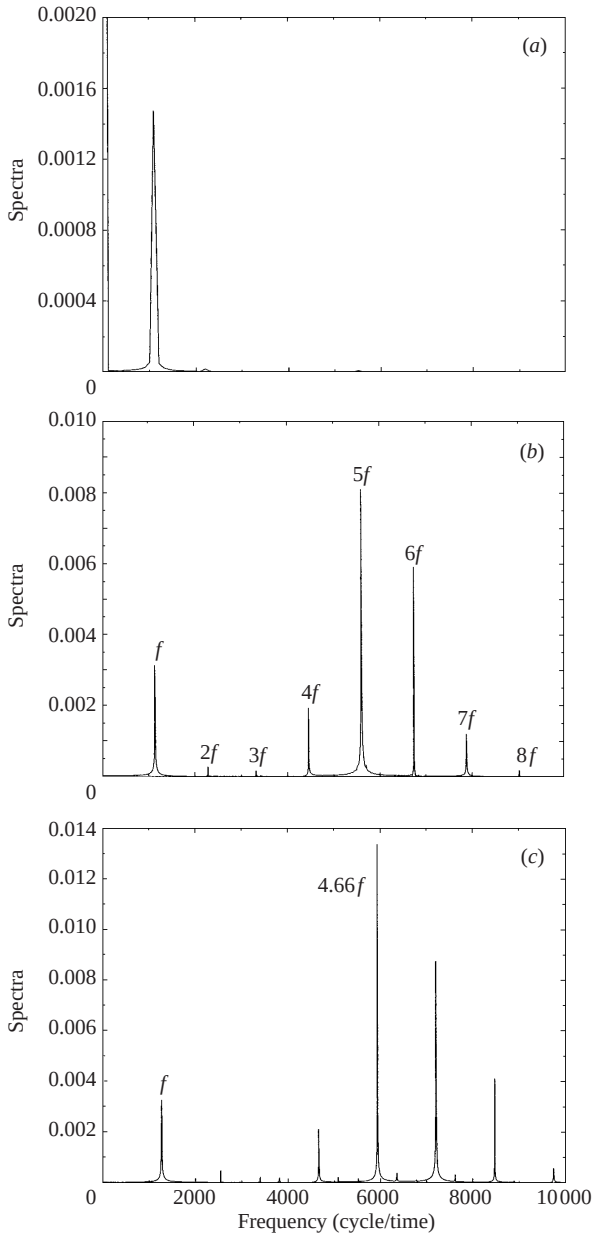

FIGURE 5. Spectra of the time series at ($x = 1/120$, $y = 0.91$) for the stratified flow at (*a*) $Ra = 0.825 \times 10^8$, (*b*) $Ra = 0.875 \times 10^8$, (*c*) $Ra = 1.0 \times 10^8$.

f_1 and f_2 can also be seen in the figure. Figure 6 shows temperature time series at $x = 1/120$ and a range of y locations for $Ra = 1.0 \times 10^8$, clearly showing the multi-modal structure of the signal.

The unsteady behaviour described above only occurs for the flow with stratified background. No such unsteady behaviour was observed for the non-stratified flow, even when the Rayleigh number was increased to $Ra = 1.0 \times 10^{10}$.

For the stratified flow the character of the higher-frequency modes that are domi-

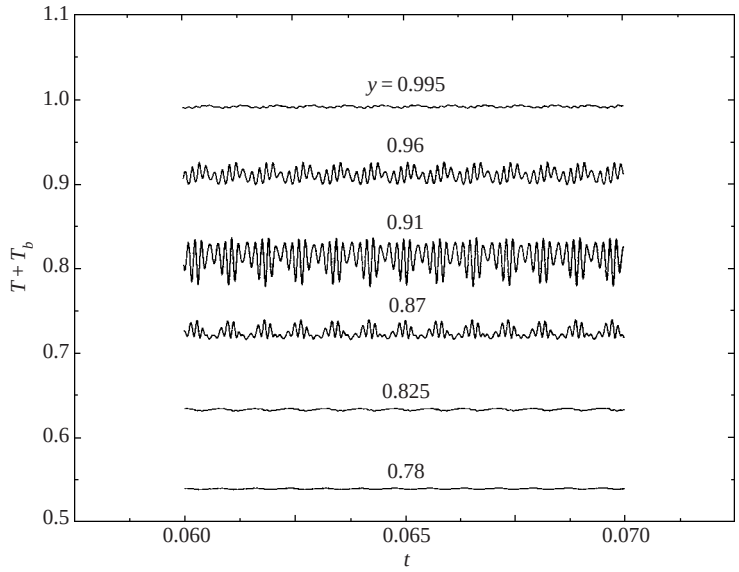

FIGURE 6. Time series of temperature at $x = 1/120$ for the stratified flow at $Ra = 1.0 \times 10^8$.

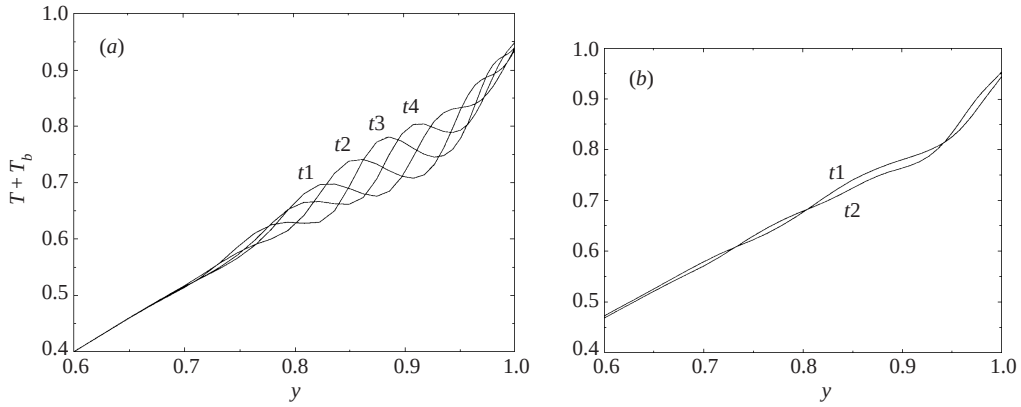

FIGURE 7. Vertical profiles for the temperature at $x = 1/120$ and (*a*) $Ra = 1.0 \times 10^8$, at times $t1 = 0.06500$, $t2 = 0.06503$, $t3 = 0.06506$, $t4 = 0.06509$; (*b*) $Ra = 0.825 \times 10^8$, at times $t1 = 0.06500$, $t2 = 0.06554$.

nant at the higher Rayleigh numbers is quite different to that of the lower frequency. Figure 7(*a*) shows the vertical profile of the temperature in the boundary layer at $x = 1/120$ from $y = 0.6$ to $y = 1.00$ at $Ra = 1.0 \times 10^8$ at four times. For this Rayleigh number the higher-frequency mode is dominant, and it is seen that this mode corresponds to a wave travelling up the boundary layer. The wave is located only in the upper region of the boundary layer and has a maximum amplitude at approximately $y = 0.9$. Figure 7(*b*) shows the equivalent result for the Rayleigh number $Ra = 0.825 \times 10^8$. At this Rayleigh number the lower-frequency mode is dominant. The difference of the two times shown is half the period of the lower-frequency mode, which is seen to correspond to a stationary perturbation of the boundary layer, again located only in the upper region with a maximum amplitude at approximately $y = 0.89$ and visible fixed nodes at $y = 0.94, 0.80, 0.73$. The amplitude of this mode

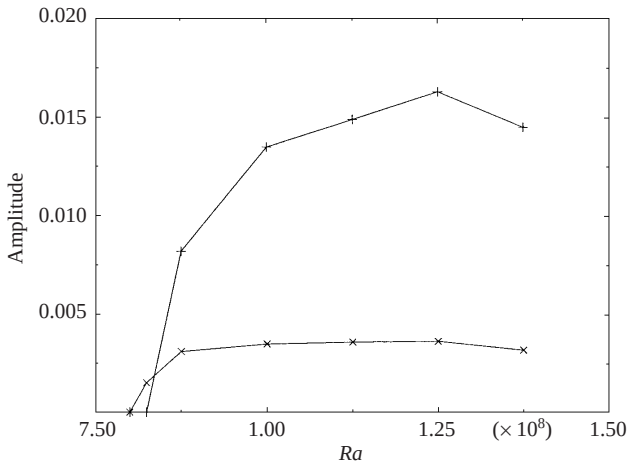

FIGURE 8. Amplitude of the low-frequency mode (×) and the dominant high-frequency mode (+) against *Ra*.

also decays rapidly for reducing y. The low-frequency amplitude is very small, of the order of 10^{-4}. To make the signal visible on figure 7(*b*) the difference between the two profiles and the time-averaged profile was magnified by a factor of 50.

It is apparent that two transitions have occurred: the first is that of the lower-frequency mode which corresponds to a stationary wave, while the second is that of the higher-frequency mode which corresponds to a travelling wave. Determining the critical Rayleigh number exactly for the occurence of each of these frequencies is difficult. Figure 8 contains the amplitude of each of the modes plotted against Rayleigh number. In this case the higher-frequency mode is chosen as the dominant higher frequency, corresponding for example to $f = 5900$ at $Ra = 1.0 \times 10^8$. These results are also presented in table 1. The lower frequency is seen to first occur between $Ra = 0.8 \times 10^8$ and $Ra = 0.825 \times 10^8$, while the higher frequency first occurs between $Ra = 0.825 \times 10^8$ and $Ra = 0.875 \times 10^8$.

As noted above, the unsteady flow occurs only with a background stratification. A major difference between the stratified and non-stratified flow is the occurrence of the reverse-S region in the former. It has also been observed that the oscillations in the boundary layer, both low and high frequency, occur only in the upper region adjacent to the reverse S. It is therefore very likely that the reverse-S shape is associated with the unsteady behaviour of the stratified flow. To test this hypothesis simulations have been obtained for a jet located in the upper left corner of the domain with the characteristics of the natural convection boundary layer exit jet. The parabolic velocity profile used for the corner jet simulation is shown in figure 9, compared to the boundary layer exit jet profile extracted directly from the computation with $Ra = 1 \times 10^8$. The exit jet profile lies on the vertical line at $x = 0.05$, which is seen in figure 3 to correspond to the location at which the streamlines exiting the boundary layer are horizontal. The corner jet was given a linear temperature profile which closely approximated that of the exit jet, as shown in figure 10, again for $Ra = 1.0 \times 10^8$

Streamfunction and temperature contour results for the corner jet, with background stratification, are shown in figure 11, where it is seen that a reverse-S structure is generated, very similar to that of the full flow. To generate this structure it was also

$Ra \times 10^{-8}$	Amplitude of dominant high freq.	Amplitude of low freq.
0.80	0	0
0.825	0	0.0015
0.875	0.0083	0.0031
1.00	0.0135	0.0035
1.125	0.0149	0.0036
1.250	0.0163	0.0035
1.375	0.0145	0.0032

TABLE 1. Amplitude of the spectra for dominant modes for the different Ra; $T_t = 1.0$, $\mathrm{d}T/\mathrm{d}y = 2$.

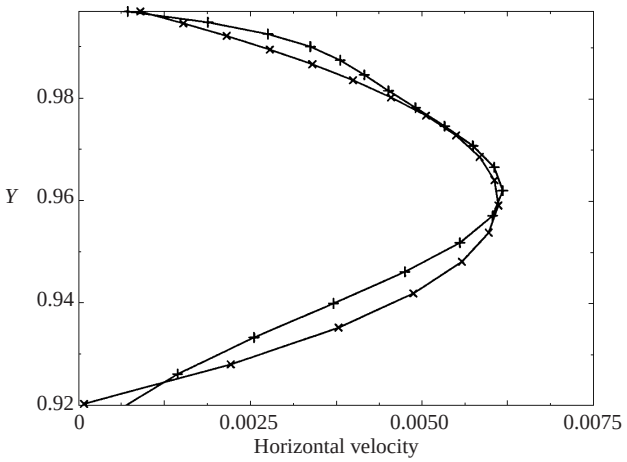

FIGURE 9. Vertical profiles of the horizontal velocity: used in corner jet simulations (×), extracted from numerical simulations (+).

necessary to specify a small region of zero buoyancy adjacent to the jet entrance, $y \geqslant 0.9$, $x \leqslant 0.08$. Without this region the corner jet turned very sharply down immediately after entering the domain, rather than following the smooth curve seen in figure 11.

Corner jet simulations were run with the standard background stratification and a range of velocity and temperature inlet profiles, corresponding to the boundary layer exit jet for Rayleigh numbers from $Ra = 0.75 \times 10^8$ to $Ra = 2 \times 10^8$. It was found that for jet and temperature profiles corresponding to $Ra \geqslant 1 \times 10^8$ the corner jet displayed a bifurcation similar to that in the full open cavity flow. Figure 12 shows temperature time series at $x = 0.1, y = 0.9$ for the corner jet with velocity and temperature profiles corresponding to the $Ra = 1.25 \times 10^8$ flow showing the oscillatory behaviour. Figure 13 contains the spectrum of the temperature time series for this case, showing that the structure is dominated by the $f = 1669$ base frequency, with clear peaks at harmonics up to five times the base frequency. Changing the characteristics of the corner jet to correspond to higher-Ra flows increases the amplitude of all the modes, but always with the lowest frequency mode dominant.

The corner jet simulation has also been run with no background stratification ($T_b = 0$). In this case the jet remains attached to the upper boundary over the full length of the domain with no reverse S and no bifurcation. Similarly running the corner jet simulation with no buoyancy over the entire domain led to no bifucation.

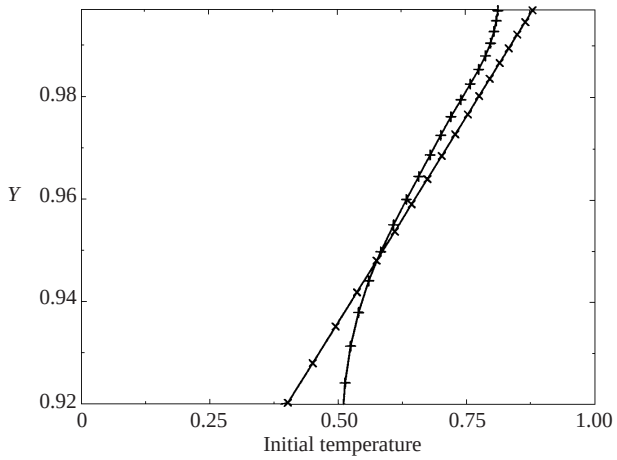

FIGURE 10. Vertical profiles of the temperature: used in corner simulations (×), extracted from numerical simulations (+).

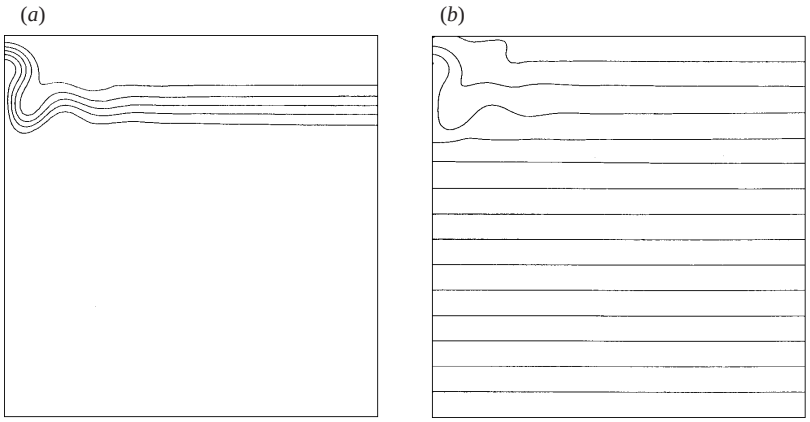

FIGURE 11. Streamfunction (*a*) and temperature (*b*) contour plots for the corner jet.

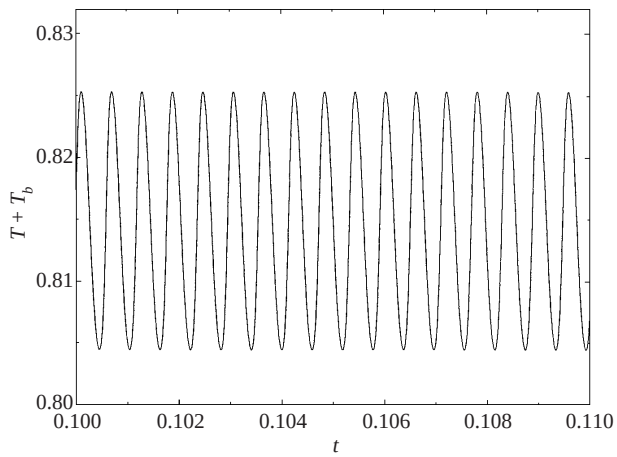

FIGURE 12. Time series of temperature at ($x = 0.1$, $y = 0.9$) for the corner jet.

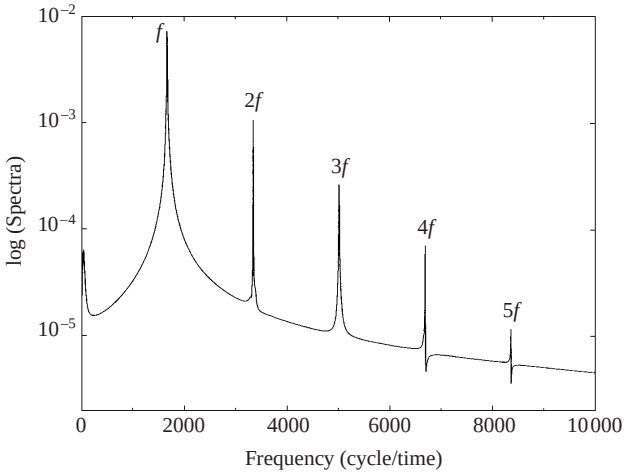

FIGURE 13. Spectra of the time series at ($x = 0.1$, $y = 0.9$) for the corner jet.

To determine the effect of the upper boundary on the flow behaviour a jet has been specified at the centre of the left-hand boundary with the same velocity characteristics as the corner jet, with a linear temperature field with a similar relation to the local background stratification as that given above when the jet is located at the upper corner of the domain, and using the standard stratification. This free jet exhibited a similar reverse-S flow and unsteady behaviour as that of the corner jet. The free jet was also tested with a linear temperature structure exactly matching the local background stratification, in which case no reverse S and no bifucation occurred. The free jet was also run with no buoyancy over the entire domain, producing a conventional plane jet. The plane jet had no reverse S, but did show unsteady behaviour with a frequency a factor of twenty less than that observed with buoyancy included and the reverse S structure present.

The other main feature of the open cavity flow is the natural convection boundary layer that forms on the heated wall, and which produces the exit jet. This flow feature has also been examined in isolation by setting the upper boundary open with zero vertical derivative in the vertical and horizontal velocities as well as temperature. With this configuration and no background stratification the boundary layer exits the domain smoothly with no unsteadiness observed at Rayleigh numbers up to $Ra = 1 \times 10^{10}$. However when the standard background temperature stratification is specified a turning flow and reverse-S shape is generated, even with the open upper boundary. Additionally, for high enough Rayleigh number low- and high-frequency signals are observed. This demonstrates that the S structure, and associated bifurcation, is generated by the background stratification alone. To test the behaviour of the natural convection boundary layer with background stratification but with no turning flow and reverse S it was necessary set the background temperature T_b at the upper boundary to 0.8. In this case the stratification gradient was maintained at 2 and the background temperature at the bottom boundary was therefore -1.2. The boundary layer then passed smoothly through the upper boundary with no turning flow and reverse S generated and no unsteadiness was observed for Rayleigh numbers up to $Ra = 1 \times 10^{10}$. Alternatively when the background stratification at the upper boundary was set to 1.2, with again the same stratification gradient, a reverse S and intrusion with exactly the same character as for the open cavity with fixed upper

$Ra \times 10^{-8}$	Low freq. f_l	$f_l/(Pr/Ra)^{-1/2}$	Dominant high freq. f_d	$f_d/(Pr/Ra)^{-2/3}$
0.80	0	0	0	0
0.825	1100	0.099	0	0
0.875	1120	0.101	5600	0.0224
1.00	1275	0.107	5936	0.0217
1.125	1392	0.110	6275	0.0212
1.250	1571	0.117	8100	0.0255
1.375	1616	0.115	8425	0.0249

TABLE 2. Observed frequencies for the different Ra; $T_t = 1.0$, $\mathrm{d}T/\mathrm{d}y = 2$.

boundary and background stratification was generated, but with the upper boundary of the exit jet at $y = 0.9$, the height at which the the heated wall temperature matched T_b. For high enough Rayleigh number this flow exhibited exactly the same unsteady behaviour as the standard open cavity with fixed upper boundary and background stratification. The critical Rayleigh number for the occurrence of the bifurcation in this case is greater than that of the standard case when the background temperature at the upper boundary is 1.0.

4. Discussion

The behaviour of the stratified open cavity flow observed here is very similar to that of the closed cavity at the same Prandtl number, discussed in the introduction. In the closed cavity the lower-frequency bifurcation has been identified as corresponding to an internal wave mode, and thus is expected to scale with $(Pr/Ra)^{1/2}$. The second, higher frequency corresponds to a boundary layer mode, and is expected to scale with $(Pr/Ra)^{2/3}$ (Janssen & Henkes 1995). In the closed cavity the critical Rayleigh number for the lower frequency is between $Ra = 0.75 \times 10^8$ and $Ra = 1.0 \times 10^8$, while that for the higher frequency is between 1.25×10^8 and 1.5×10^8 (these Rayleigh numbers are expressed in terms of the boundary layer temperature difference to conform with the definition used in this paper; Janssen & Henkes gave values in terms of the total temperature difference for the closed cavity which are twice those given here). Again in the closed cavity the scaled lower frequency, at bifurcation, is

$$f_l/(Pr/Ra)^{-1/2} = 0.073$$

and the scaled higher frequency is

$$f_h/(Pr/Ra)^{-2/3} = 0.032.$$

Closed cavity simulations have also been carried out as part of the current investigation and it has been observed that the lower-frequency mode corresponds to a stationary oscillation located predominantly at the upper part of the heated wall (and lower part of the cooled wall), and the higher frequency mode corresponds to a travelling wave again located only at the upper part of the heated wall (and lower part of the cooled wall).

Rayleigh number, and scaled and unscaled lower and higher frequencies for the stratified open cavity are presented in table 2. It is seen that the correspondence of these results with those of the closed cavity is good, although not exact. The critical Rayleigh number for the lower frequency is between $Ra = 0.8 \times 10^8$ and

$Ra \times 10^{-8}$	Low freq. f_l	$f_l/(Pr/Ra)^{-1/2}$
0.750	0	0
0.825	0	0
0.875	0	0
1.000	1493	0.125
1.125	1607	0.126
1.250	1669	0.125
1.500	1707	0.117
1.750	1851	0.117
2.000	1966	0.116

TABLE 3. Observed frequencies for the different Ra; $Tt = 1.0$, $\mathrm{d}T/\mathrm{d}y = 2$.

$Ra = 0.825 \times 10^8$, very close to that of the closed cavity. The critical Rayleigh number for the higher frequency is between $Ra = 0.825 \times 10^8$ and $Ra = 0.875 \times 10^8$, slightly lower than that of the closed cavity. The scaled lower frequency at bifurcation is 0.099, slightly higher than the closed cavity, while the scaled higher frequency at $Ra = 0.875 \times 10^8$ is 0.0224, slightly lower than that of the closed cavity. The stratified open cavity flow is not identical to the closed cavity flow, and therefore exact numerical agreement cannot be expected. However it is clear that they are qualitatively similar, with reasonable quantitative agreement, and it is expected that the underlying fluid mechanics and generation mechanisms for the bifurcation are identical.

In the previous section it was demonstrated that the bifurcation is closely associated with the reverse-S structure. The lack of this structure in the homogeneous open cavity flow is the most likely reason that no bifurcation occurs there. In previous work on the closed cavity, which exhibits an identical reverse-S flow, it was suggested that the lower frequency is a result of an instability of the exit jet at the downstream end of the thermal boundary layer on the heated (and cooled) wall, in analogy with the known instability of the Bickley jet (Janssen & Henkes 1995). The localization of the lower-frequency signal to the upper region of the heated plate in the open cavity flow again suggests that it is an instability in this region that generates the lower frequency. An extensive investigation of the boundary layer exit jet has been carried out by specifying a jet at the upper corner of the left-hand boundary with the same velocity and temperature characteristics as those of the exit jet in the open cavity flow. This jet, with the standard background stratification exhibits the same reverse-S structure as the open cavity natural convection flow with background stratification. The corner jet also exhibited a bifurcation when the jet profile and temperature corresponded to those of the boundary layer exit jet for a Rayleigh number greater than 1×10^8. As the Rayleigh number was further increased additional higher-frequency signals appeared, initially as harmonics but then as a broadbanded signal; however the lowest frequency always remained dominant. Table 3 lists the low frequencies obtained with the corner jet scaled with the internal wave mode. These values are close to those of the low frequency for the full natural convection open cavity flow, given in table 2, and it is very likely that the generation mechanism for the corner jet bifucation is the same as that for the low frequency in the open cavity.

The corner jet with either no background stratification or no buoyancy results in an attached wall jet with no S structure and no unsteadiness. Furthermore it was

found that for the corner jet the reverse-S flow and bifurcation were dependent on the presence of the upper boundary. Exactly the same behaviour was observed when the jet was located at the centre of the left-hand boundary, provided the jet temperature had the same relation to the local background temperature as that of the corner jet. If the centre jet temperature was set to exactly match the background temperature a free jet, with no S shape and no unsteadiness, was generated. Finally the centre jet with no buoyancy generated a standard plane jet. Such plane jets are known to exhibit unsteady behaviour for high enough entrance Reynolds number as a result of a Kelvin–Helmholtz instability on the double shear layers and such behaviour was observed here, with a frequency one-twentieth of that observed when buoyancy, stratification and the reverse-S flow are all present.

These results make it clear that the low-frequency bifurcation signal is fully correlated with the S structure. The effect of the S structure at the corner is to shift the exit jet away from the upper boundary, producing a free jet. This feature was also observed in the closed cavity by Janssen & Henkes (1995) who suggested that the low-frequency bifurcation was a result of a shear instability of this free jet, and showed that the low-frequency signal was predominantly shear generated. The results obtained here provide support for their hypothesis.

The reverse-S structure was examined in detail in the context of the closed cavity flow by Ravi *et al.* (1994), where it was shown that the flow was generated by a thermal mechanism for Rayleigh numbers $Ra > 1\times10^6$. The reverse-S structure in the stratified open cavity has the same generation mechanism, which is as follows: The exit jet has approximately the same temperature structure as the natural convection boundary layer with the upper boundary temperature slightly below that of the heated wall as a result of the zero-gradient boundary condition on the upper boundary. Similarly the temperature of the lower part of the jet is less than that of the adjacent ambient fluid as a result of entrainment. The temperature gradient within the jet is considerably greater than that of the background stratification. Buoyancy forces then act to shift each fluid particle within the jet to a position of neutral buoyancy with respect to the background stratification, leading to a shift of the jet away from the upper boundary, the thickening of the jet and the generation of the reverse-S structure.

It is well known that natural convection boundary layers are convectively unstable to a narrow band of modes when the Rayleigh number is above a critical value of about $Ra = 1 \times 10^5$. Applying a perturbation, with a frequency within the amplifying band, to the natural convection boundary layer produces a train of waves travelling downstream from the point of perturbation, amplifying as they travel. The second dominant higher frequency in the bifurcated cavity flow corresponds approximately to the most unstable mode for the natural convection boundary layer in the upper region of the wall (Janssen & Armfield 1996), and it is clear that these waves are associated with this known instability of the boundary layer. However, many of the features of the higher-frequency waves do not correspond to the known characteristics of the boundary layer instability. A continuous perturbation at the appropriate mode is necessary to generate the boundary layer waves, and no such perturbation is evident in the cavity system. If the waves were the result of small background perturbations then there is no reason for them to be localized to the downstream region of the boundary layer irrespective of the Rayleigh number. The point at which the waves become unstable would be expected to move upstream as the Rayleigh number is increased. This behaviour is observed in neither the open or closed cavity flows. Finally no unsteadiness is observed in the pure boundary layer flow with open upper boundary, with and without background stratification, unless the reverse S is generated.

Results obtained with the corner jet showed that when the jet velocity profile and temperature structure correspond to a thermal boundary layer exit jet with a Rayleigh number above a critical value, the flow bifurcates with a frequency approximately the same as that of the lower frequency in the standard open cavity flow with stratification. The corner jet flow above the critical Rayleigh number also contains harmonics of the base frequency. As the Rayleigh number is increased the amplitude of the base frequency and harmonics increases, with the additional higher-frequency modes appearing to produce a broadbanded signal. However in the Rayleigh number range considered the low-frequency amplitude always dominated that of the higher frequencies. Results for the standard open cavity flow showed that the dominant high-frequency signal occurs initially as a harmonic with five times the frequency of the base low-frequency mode. This behaviour suggests that the convectively unstable boundary layer is selectively amplifying modes already present as harmonics of the low-frequency signal associated with the reverse-S structure.

Previous researchers have noted that no bifurcation occurs for the closed cavity with Prandtl number $Pr = 7$. In the present study open cavity flow with background stratification and $Pr = 7$ has also been investigated, and no bifurcation was observed. In the higher Prandtl number flow the velocity boundary layer is thicker than the thermal boundary layer, and consequently no strong exit jet and no associated reverse-S structure is generated. There is then no jet instability and therefore no bifucation is expected.

5. Conclusions

A two-dimensional finite-volume model has been used for the prediction of Prandtl number $Pr = 0.7$ flow in an open cavity with heated sidewall, with and without background stratification. The flow without background stratification is composed of a thermal boundary layer entraining ambient fluid over most of its height which is discharged as a jet at the downstream end of the boundary layer. The jet travels across the cavity beneath the upper boundary and exits through the open boundary with little change in character.

The flow with background stratification entrains fluid only over the upstream half of the boundary layer, and the exit jet forms a tight reverse-S shape at the downstream end of the boundary layer, discharging into a thick intrusion that travels across the cavity and exits through the open boundary. The character of the downstream flow with stratified background is quite different to that of the flow with homogeneous background. The homogeneous flow is steady at large time, whereas the stratified flow at high enough Rayleigh number exhibits a bifurcation with characteristic low and high frequencies of the same type as observed for closed cavity flow.

Simulations for a corner jet and a free centre jet, with velocity and temperature profiles approximately the same as those of the boundary layer exit jet, showed that the low frequency is associated with an instability of the reverse-S flow structure, which itself results from the buoyancy interaction between the jet temperature field and the local background temperature field. A free plane jet with the same initial velocity profile and no buoyancy also exhibits an instability, but with a frequency a factor of twenty less than that of the reverse-S flow. It is very likely that the shear mechanism leading to the instability of the free plane jet is the same as that leading to the instability of the reverse S; however the large difference in frequency indicates a substantial modification as a result of buoyancy and streamline curvature.

The corner jet with reverse-S flow structure, at high enough Rayleigh number,

exhibits multi-modal behaviour with harmonics visible up to at least five times the base frequency, but with the base signal always dominating the power spectrum. This is similar to the standard natural convection open cavity flow with background stratification, which also exhibits harmonics of the base frequency. However for the natural convection open cavity flow the harmonics quickly dominate the base frequency. The natural convection boundary layer is known to be convectively unstable to a narrow band of frequencies and it is very likely that the boundary layer is selectively amplifying the harmonics, which then dominate the base frequency. It therefore appears that both the low- and high-frequency signals result from the bifurcation of the free jet associated with the formation of the reverse-S flow.

This work was supported by the Australian Research Council under grants A89600146 and A89701794. Useful conversations with John Patterson are also acknowledged.

REFERENCES

Armfield, S. W. & Janssen, R. J. A. 1996 A direct boundary-layer stability analysis of steady-state cavity convection flow. *Intl J. Heat Fluid Flow* **17**, 539–546.

Armfield, S. W. & Patterson, J. C. 1992 Wave properties of of natural convection boundary layers. *J. Fluid Mech.* **239**, 195–211.

Armfield, S. W. & Street, R. 1999 Fractional step methods for the navier-stokes equations in staggered grids: the accuracy of three variations. *J. Comput. Phys.* (in press).

Bejan, A. & Kimura, A. 1981 Penetration of free convection into a lateral cavity. *J. Fluid Mech.* **103**, 465–478.

Chan, Y. L. & Tien, C. L. 1985 A numerical study of two-dimensional laminar natural convection in shallow open cavities. *Intl J. Heat Mass Transfer* **28**, 603–612.

Gill, A. E. & Davey, A. 1969 Instabilities of a buoyancy-driven system. *J. Fluid Mech.* **35**, 775–798.

Han, T. Y., Meng, J. C. S. & Innis, G. E. 1983 An open boundary condition for incompressible stratified flows. *J. Comput. Phys.* **49**, 276–297.

Hartnett, J. P. & Welsh, W. E. 1957 Experimental studies of free convection heat transfer in a vertical tube with uniform wall heat flux. *Trans. ASME* **79**, 1551–1557.

Janssen, R. J. A. & Armfield, S. W. 1996 Stability properties of the vertical boundary layers in differentially heated cavities. *Intl J. Heat Fluid Flow* **17**, 547–556.

Janssen, R. J. A. & Henkes, R. A. W. M. 1995 Influence of prandtl number on instability mechanisms and transitions in a differentially heated square cavity. *J. Fluid Mech.* **290**, 319–344.

Japikse, D. 1973 Advances in thermosyphon technology. *Adv. Heat Transfer* **9**, 8–40.

Javam, A. 1995 Role of internal waves in subsurface mixing. PhD thesis, University of Western Australia.

Leonard, B. P. 1979 A stable and accurate convective modelling procedure based on quadratic upstream interpolation. *Comput. Meth. Appl. Mech. Engng* **19**, 59–98.

Le Quere, P. & Alziary de Roquefort, T. 1985 Transition to unsteady natural convection of air in differentially heated vertical cavities. *4th Intl Conf. on Numerical Methods in Laminar and Turbulent Flow*, vol. 4, pp. 841–852.

Le Quere, P. & Behnia, M. 1998 From onset of unsteadiness to chaos in a differentially heated square cavity. *J. Fluid Mech.* **359**, 81–107.

Le Quere, P., Humphrey, J. A. C. & Sherman, F. S. 1981 Numerical calculation of thermally driven two-dimensional unsteady laminar flow in cavities of rectangular cross section. *Numer. Heat Transfer* **4**, 249–283.

Lighthill, M. J. 1953 Theoretical considerations on free convection in tubes. *Q. J. Mech. Appl. Maths* **6**, 398–439.

Mohamad, A. A. 1995 Natural convection in open cavities and slots. *J. Numer. Heat Transfer* A **27**, 705–716.

Paolucci, S. & Chenoweth, D. R. 1989 Transition to chaos in a differentially heated vertical cavity. *J. Fluid Mech.* **201**, 379–410.

Patterson, J. C. & Armfield, S. W. 1990 Transient features of natural convection in a cavity. *J. Fluid Mech.* **219**, 469–498.

Penot, P. 1982 Numerical calculations of two-dimensional natural convection in isothermal open cavities. *Numer. Heat Transfer* **5**, 21–437.

Ravi, M. R., Henkes, R. A. W. M. & Hoogendoorn, C. J. 1994 On the high Rayleigh number structure of steady laminar natural convection flow in a square enclosure. *J. Fluid Mech.* **262**, 325–351.